PNAS RESEARCH ARTICLE | MEDICAL SCIENCES

Rhabdomyosarcomas are oncogene addicted to the activation of AVIL

Zhongqiu Xie[a], Pawel L. Janczyk[a], Xinrui Shi[b], Qiong Wang[a,c], Sandeep Singh[a], Robert Cornelison[a], Jingjing Xu[a,d], James W. Mandell[a], Frederic G. Barr[e], and Hui Li[a,b,1]

Edited by Jerry Adams, Walter and Eliza Hall Institute of Medical Research, Melbourne, Victoria; received October 1, 2021; accepted March 11, 2022

Rhabdomyosarcoma (RMS) is one of the most common pediatric soft-tissue cancer. Previously, we discovered a gene fusion, *MARS-AVIL* formed by chromosomal inversion in RMS. Suspecting that forming a fusion with a housekeeping gene may be one of the mechanisms to dysregulate an oncogene, we investigated AVIL expression and its role in RMS. We first showed that MARS-AVIL translates into an in-frame fusion protein, which is critical for RMS cell tumorigenesis. Besides forming a gene fusion with the housekeeping gene, *MARS*, the AVIL locus is often amplified, and its RNA and protein expression are overexpressed in the majority of RMSs. Tumors with AVIL dysregulation exhibit evidence of oncogene addiction: Silencing MARS-AVIL in cells harboring the fusion, or silencing AVIL in cells with AVIL overexpression, nearly eradicated the cells in culture, as well as inhibited in vivo xenograft growth in mice. Conversely, gain-of-function manipulations of AVIL led to increased cell growth and migration, enhanced foci formation in mouse fibroblasts, and most importantly transformed mesenchymal stem cells in vitro and in vivo. Mechanistically, AVIL seems to serve as a converging node functioning upstream of two oncogenic pathways, PAX3-FOXO1 and RAS, thus connecting two types of RMS associated with these pathways. Interestingly, AVIL is overexpressed in other sarcoma cells as well, and its expression correlates with clinical outcomes, with higher levels of AVIL expression being associated with worse prognosis. *AVIL* is a bona fide oncogene in RMS, and RMS cells are addicted to its activity.

rhabdomyosarcoma | MARS-AVIL | AVIL | oncogene

Significance

Rhabdomyosarcoma (RMS) is a common pediatric soft-tissue cancer. There are two main subtypes driven by distinct mechanisms. Currently, there is no targeted therapy for the disease. We found an oncogene AVIL, whose activity is often abnormally up-regulated in RMS. Silencing the gene kills RMS cells and prevents tumor formation in animals; yet, normal control cells are indifferent to the interference. Mechanistically, AVIL activation turns on both oncogene pathways in RMS. These findings support that AVIL may be a good therapeutic target and that targeting AVIL may be a viable approach for both types of RMS.

Rhabdomyosarcoma (RMS) is one of the most common soft-tissue cancer in children, adolescents, and young adults (<20 y old). Of the various subtypes of RMS, embryonal (ERMS) and alveolar rhabdomyosarcomas (ARMS) are the most commonly encountered (1). Recent studies have revealed that PAX3/7-FOXO1 fusions are crucial for ARMS, which are also called fusion-positive RMS. PAX3/7-FOXO1 fusion-negative ARMS are clinically and molecularly indistinguishable from ERMS (2–4); thus, they are grouped now as fusion-negative RMS. Despite collaborative national trials of multimodal therapy and chemotherapy intensification, the outcome for patients with advanced-stage RMS has not improved in two decades (around 27% survival at 3 y) (5, 6). As of now, no targeted therapy is available.

AVIL encodes the protein advillin, which is a member of the gelsolin/villin family of actin regulatory proteins (7). Previously, we identified a gene fusion that joins AVIL with a housekeeping gene *MARS* (methionyl-tRNA synthetase) in ARMS (8, 9). Given that many gene fusions often activate one of the parental genes as a protooncogene and produce oncogenic fusion protein, we hypothesized that the MARS-AVIL fusion and, more importantly, AVIL gene itself might play oncogenic roles in RMS tumorigenesis. Indeed, the *AVIL* locus is often amplified, and more frequently, AVIL RNA and protein are overexpressed in RMS cell lines, patient-derived xenografts (PDXs), and clinical samples. Functionally, AVIL is critical for RMS cells with AVIL overexpression, as its silencing resulted in a dramatic reduction of proliferation and migration. Yet, it is dispensable for the control of mesenchymal stem cells (MSCs). Classic focus formation assay and transformation in vivo proved that AVIL is a bona fide oncogene. Mechanistically, AVIL affects both PAX-FOXO1 fusion and RAS targets and may serve as a convergent node for ARMS and ERMS oncogenic signaling pathways.

Results

MARS-AVIL Fusion Encodes a Fusion Protein in RMS. Through paired-end RNA sequencing (RNA-seq), we identified in RH30 (RMS cell line), a fusion transcript joining the first 10 exons of *MARS* (methionyl-tRNA synthetase) to the last 15 exons of *AVIL* (advillin) (Fig. 1 *A* and *B*). Surprisingly, even though *PAX3-FOXO1* is the most

Author affiliations: [a]Department of Pathology, School of Medicine, University of Virginia, Charlottesville, VA 22908; [b]Department of Biochemistry and Molecular Genetics, School of Medicine, University of Virginia, Charlottesville, VA 22908; [c]Department of Urology, Guangdong Provincial Key Laboratory of Malignant Tumor Epigenetics and Gene Regulation, Sun Yat-Sen Memorial Hospital, Sun Yat-Sen University, Guangzhou 510120, China; [d]Department of Obstetrics and Gynecology, Tongji Hospital, Tongji Medical College, Huazhong University of Science and Technology, Wuhan 430030, China; and [e]Laboratory of Pathology, National Cancer Institute, Bethesda, MD 20892

Author contributions: Z.X. and H.L. designed research; Z.X., P.L.J., X.S., Q.W., and J.X. performed research; F.G.B. contributed new reagents/analytic tools; Z.X., P.L.J., X.S., Q.W., S.S., R.C., J.X., J.W.M., and H.L. analyzed data; and Z.X. and H.L. wrote the paper.

The authors declare no competing interest.

This article is a PNAS Direct Submission.

[1]To whom correspondence may be addressed. Email: hl9r@virginia.edu.

This article contains supporting information online at http://www.pnas.org/lookup/suppl/doi:10.1073/pnas.2118048119/-/DCSupplemental.

Published June 6, 2022.

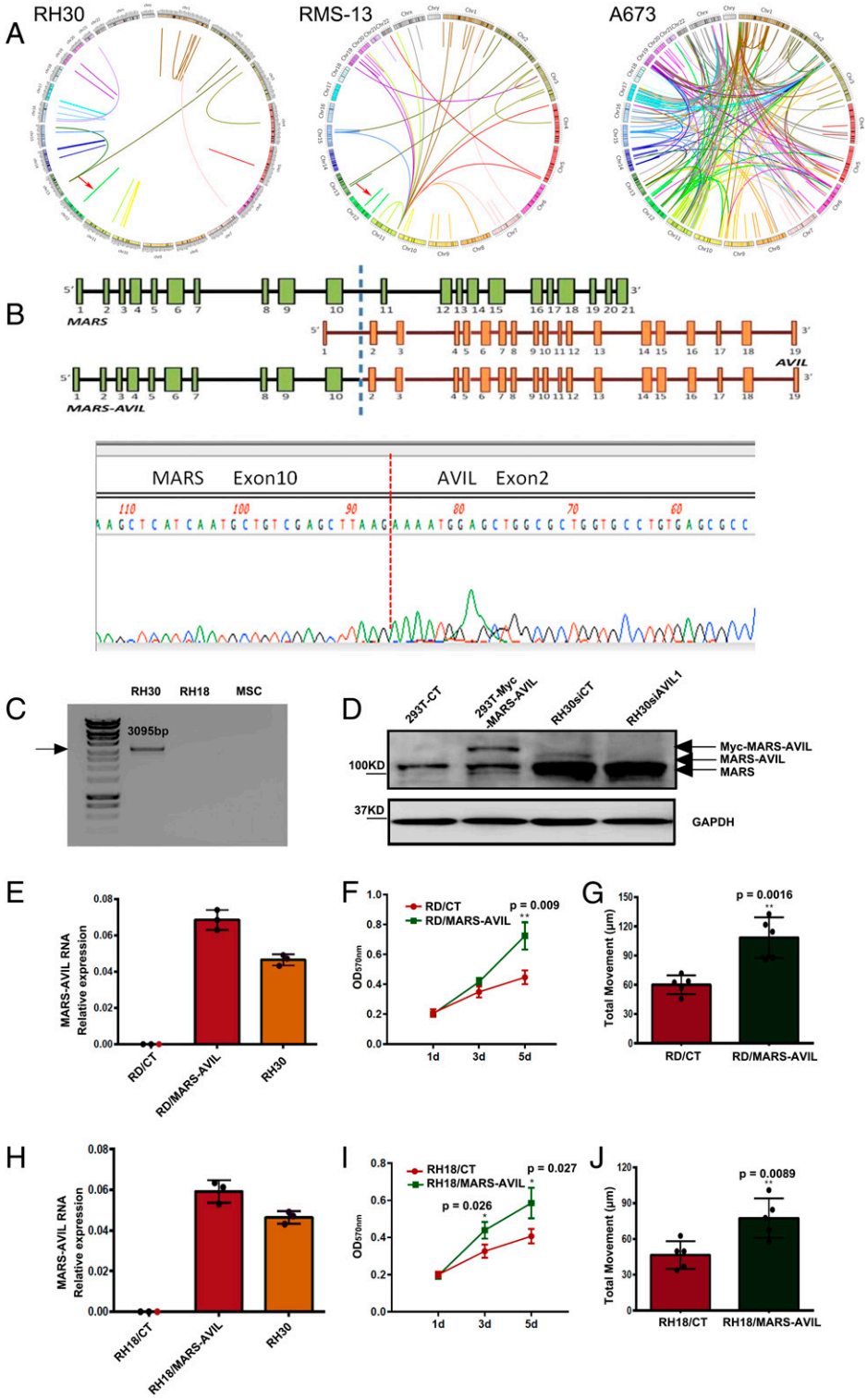

Fig. 1. MARS-AVIL fusion in RMS. (*A*) Circos plot showing fusion transcripts discovered in RH30, RMS13, and A673 sarcoma cells. Each line connects the parental genes in the genome. (*B*) The fusion is composed of the first 10 exons of *MARS* and the last 15 exons of *AVIL*. *Lower* shows a Sanger sequencing result of the fusion RNA. The blue dotted line indicates the junction site. (*C*) Long-range PCR was used to amplify the genomic DNA fragment spanning exon10 of *MARS* and exon2 of *AVIL* in RH30 cells, but not in RH18 or MSC cells. (*D*) Western blot using MARS antibody identifying both MARS and MARS-AVIL in RH30 cells. 293T transfected with Myc-tagged MARS-AVIL was included as a control. The band corresponding to MARS-AVIL was further confirmed by siAVIL1 silencing the fusion. (*E–G* and *H–J*) Stable RD (*E*) and RH18 (*H*) cells expressing MARS-AVIL to a similar level as in RH30. (*F* and *I*) Cell proliferation measured by 3-(4,5-dimethylthiazol-2-yl)-2,5-diphenyl-2H-tetrazolium bromide (MTT) was enhanced in RD (*F*) and RH18 (*I*) cells stably expressing MARS-AVIL. (*G* and *J*) Cell motility measured by wound healing was enhanced in RD (*G*) and RH18 (*J*) cells stably expressing MARS-AVIL. Data are presented as mean values ± SD in *E–J*. *P* value was calculated by standard two-tailed *t* test. $*P < 0.05$, $**P < 0.01$.

well-known fusion in the rhabdomyosarcomas of this type (ARMS), *MARS-AVIL* has the highest number of reads (*SI Appendix*, Fig. S1*A*). The same MARS-AVIL fusion was also found in RMS13, which is thought to be derived from the same donor (10), although it has a different fusion RNA profile from RH30 (Fig. 1*A*). Other RMS lines, RH4, RH18, RD, and an Ewing sarcoma line A673, as well as fetal and adolescent muscles, do not harbor the same fusion (Fig. 1*A* and

SI Appendix, Fig. S1*B*). The *MARS* and *AVIL* genes are located in the same chromosomal region, 12q14, with 300 kb and about 15 genes separating them. They transcribe in a head-to-head configuration. Using long-range PCR, we determined that the fusion transcript results from an inversion of a fragment covering exon10 of *MARS* and exon1 *of AVIL* (Fig. 1*B*), resulting in a head-to-tail configuration. With Sanger sequencing, we pinpointed the break site, which is located in intron9 of *MARS* and intron1 of *AVIL* (*SI Appendix*, Fig. S1*C*). Long-range PCR amplified the rearranged fragment in RH30, but not in another rhabdomyosarcoma cell line, RH18, or a MSC culture (Fig. 1*C*). Interestingly, an image clone BC004134 (11), with a 100% match to the fusion junction, has been deposited in the human non-reference RNA database. It was labeled as an "mRNA similar to advillin," and the tissue source was "rhabdomyosarcoma," indicating that the fusion transcript was found independently before, just not recognized as a fusion from a chromosomal rearrangement.

The reading frame of the *AVIL* portion is the same as the *MARS* portion, predicting that the fusion transcript will translate into an in-frame chimeric protein. Using a MARS antibody, we detected a correctly sized protein as the possible fusion protein. To prove the identity of the band, we used a siRNA targeting the 3′ of *AVIL*, which silenced both *AVIL* and *MARS-AVIL* (*SI Appendix*, Fig. S2*A*) and detected the reduction of the *MARS-AVIL* protein signal with the MARS antibody. The same antibody also detected a Myc-tagged MARS-AVIL fusion in a 293T system (Fig. 1*D*).

To investigate the role of MARS-AVIL fusion in RMS, we generated RD and RH18 cells (both negative for MARS-AVIL) that stably express the fusion to a level similar to that of RH30 (Fig. 1 *E* and *H*). In both cell types, the fusion-transfected cells had significantly higher growth rates (Fig. 1 *F* and *I*) and motility measured by wound-healing assays (Fig. 1 *G* and *J*). In contrast, we overexpressed wild-type MARS in the same two lines and observed no statistically significant difference in cell growth and migration (*SI Appendix*, Fig. S3).

MARS-AVIL Is Necessary for RH30 Tumorigenesis In Vitro and In Vivo. To further investigate the implications of the MARS-AVIL fusion and complement the above gain-of-function study, we conducted loss-of-function experiments. Due to the junction sequence constraint, we could not design a fusion-specific siRNA. To overcome the hurdle, we designed two siRNAs, one targeting both the fusion and wild-type *AVIL* (siAVIL1), the other only targeting wild-type *AVIL* (siAVIL2) (*SI Appendix*, Fig. S2*A*). When RH30 cells were transfected with siAVIL1, but not siAVIL2, we noticed a dramatic reduction in cell number, which is reflected by a significant increase in the subG1 peak in cell cycle analysis (Fig. 2*A*). Consistently, we observed increased cleaved PARP and cleaved Caspase3 signals in cells transfected with siAVIL1, but not with siAVIL2 (Fig. 2*B*). Most RH30 cells died when transfected with siAVIL1 reflected by crystal violet staining (Fig. 2*C*). In addition to cell death, early time point after siAVIL1 transfection resulted in slower migration, as demonstrated by a wound-healing assay (Fig. 2*D*) and tracking of individual cells by live-cell imaging (Fig. 2 *E* and *F*). The same effect on cell number was also seen with an shRNA targeting AVIL (Fig. 2 *G* and *H*). To further rule out off-target effects of siAVIL1 and confirm that the phenotype was due to the silencing of the fusion, but not the wild-type AVIL, we performed rescue experiments. Even though not all the cells got transfected, MARS-AVIL, but not the AVIL expression vector, had a partial rescue of cell growth caused by siAVIL1 (*SI Appendix*, Fig. S2*B*). In an in vivo system, we performed subcutaneous xenografts of RH30 cells either infected with viruses expressing shAVIL1 or control shCT. Injections with shCT-infected RH30 cells resulted in tumor formation every time ($n = 10$), whereas injections with shAVIL1 yielded the appearance of only two comparatively smaller tumors (Fig. 2*I*). Consistently, tumor weight and volume comparisons between the two groups showed dramatic differences (Fig. 2 *J* and *K*). All of the mice in the control group died or reached the limit for tumor burden and had to be killed before 60 d. None of the mice in the shAVIL1 group died as a result of their tumors or had a tumor reaching the size limit (one mouse was purposely killed as a control when the first shCT mice were terminated) (Fig. 2*L*).

Considering that the shAVIL stably infected cells already proliferated slower than the control cells before injection, we constructed a tetracycline (tet)-inducible system. We acquired three tet-inducible shRNAs against AVIL from transOMIC. They are in a pZIP-TRE3G backbone, which contains a ZsGreen reporter and a puromycin-resistant gene. We then established stable cell lines expressing all three shRNAs and demonstrated that the GFP expression can be successfully induced by doxycycline (example in *SI Appendix*, Fig. S4*A*). Consistently, AVIL was silenced with doxycycline (*SI Appendix*, Fig. S4*B*). We then injected RH30 cells, which stably express one such shAVIL or shCT, subcutaneously into nude mice. The animals were fed with doxycycline-containing or control water. We observed significant reduction of tumor weight and volume in the shAVIL group only in the presence of doxycycline, but not in the shCT group (Fig. 2 *M*–*Q*).

AVIL Is Overexpressed in Other RMS Cells. We speculated that forming the gene fusion with a 5′ housekeeping gene is one way to up-regulate AVIL, and AVIL may be dysregulated by other mechanisms. It is known that the 12q13-15 locus is frequently amplified in multiple tumor types, including RMS (12). Consistently, we observed copy number gain in several RMS lines using an AVIL probe in fluorescence in situ hybridization (FISH) (Fig. 3*A*). Numerous dots in RMS13 cells indicate that either the fusion or the wild-type AVIL or both are amplified. In addition to the copy number gain, AVIL is overexpressed transcriptionally. We found that *AVIL* is overexpressed in the majority of RMS cell lines of both embryonal and alveolar histology by qRT-PCR (Fig. 3*B*). At the protein level, RMS lines regardless of ERMS or ARMS, express a higher level of AVIL than MSCs (Fig. 3*C*).

We also obtained a variety of PDX cultures from St. Jude Children's Research Hospital (13), including two PAX3-FOXO1 positives, one PAX7-FOXO1 positive, and two PAX3/7 fusion-negative samples (*SI Appendix*, Fig. S5*A*). All the PDX cells had higher expression of AVIL compared to MSCs and a fetal muscle biopsy, measured by qRT-PCR (Fig. 3*D*). Finally, we confirmed AVIL overexpression in our collection of a clinical cohort, regardless of their PAX3/7 fusion status (Fig. 3*E* and *SI Appendix*, Fig. S5*B*).

AVIL Overexpression Is Necessary for the Tumorigenesis of RMS. Next, we directly tested whether the overexpression of AVIL is required for the tumorigenesis of RMS. In cell lines, RD and SMS-CTR, which express a relatively higher level of AVIL, silencing AVIL with two different siRNAs wiped out the culture (Fig. 4 *A*–*C*). In contrast, no detrimental effect was observed with either of the siRNAs in MSC cells with low AVIL expression (Fig. 4*D*). Using live-cell imaging, we tracked individual cells at the early time point after transfection and observed significant reduction with siAVIL in cell motility in RD and SMS-CTR cells (Fig. 4 *E* and *F* and *SI Appendix*, Fig. S6). In

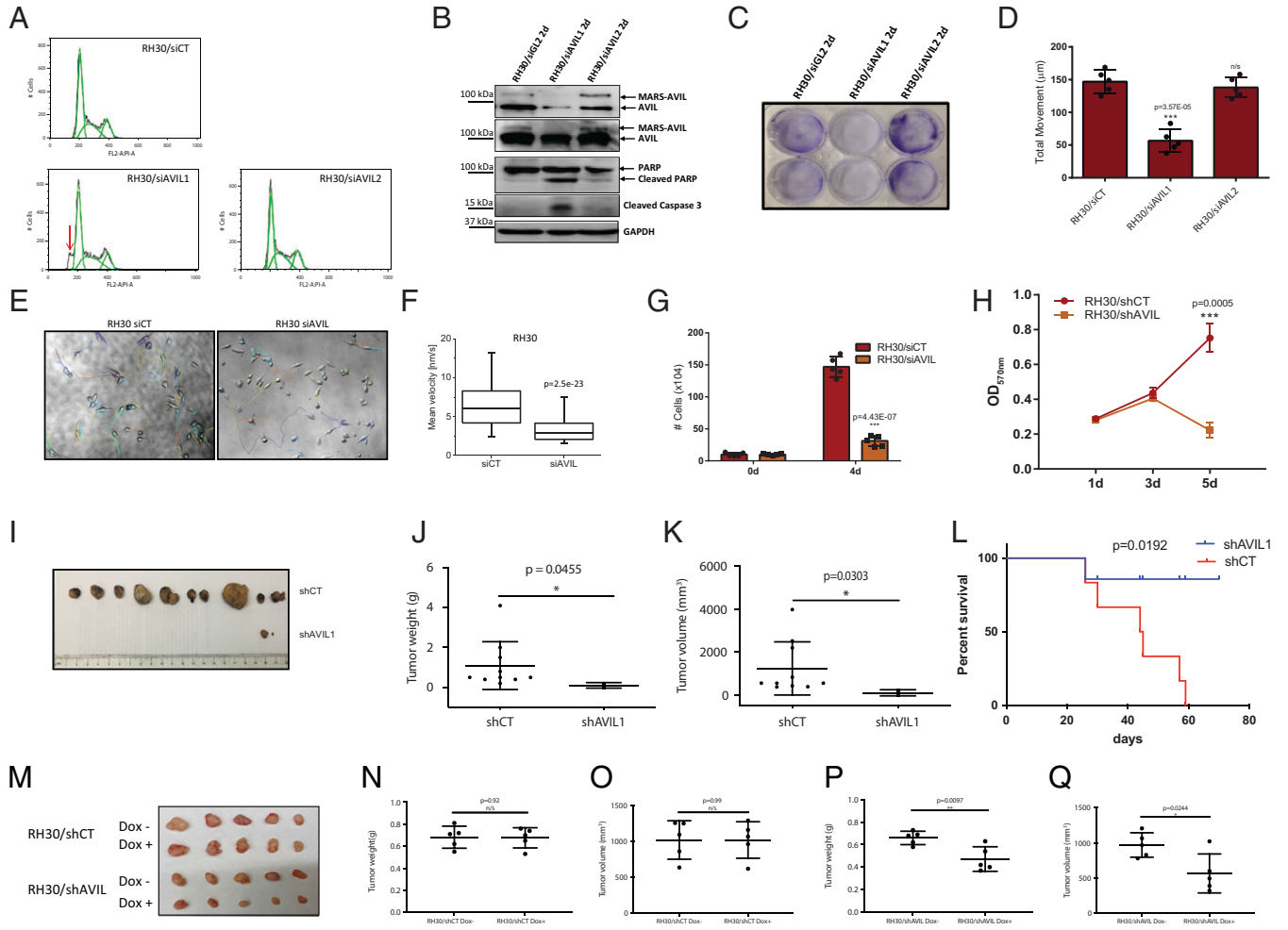

Fig. 2. MARS-AVIL is necessary for tumorigenesis in RH30 cells. (*A*) RH30 cells transfected with siAVIL1, but not siAVIL2, resulted in a sub G1 peak by flow cytometry. (*B*) Western blot using PARP and cleaved Caspase3 antibodies detected cleaved PARP and Caspase3 in RH30 cells transfected with siAVIL1, but not siAVIL2. (*C*) Crystal violet staining showed that most RH30 cells died when transfected with siAVIL1, but not siAVIL2. (*D*) RH30 cells with siAVIL1, but not siAVIL2, resulted in slower migration demonstrated by a wound-healing assay. (*E*) Live-cell tracking at an early time point of siAVIL1 transfection showed slowed cell migration compared with siCT. (*F*) Mean velocities of all cells tracked in the experiment ($n > 120$ cells quantified per condition) (box, 25 to 75 percentile; whisker, 5 to 95 percentile; bar in the *Middle*, median) (two-sided Student's *t* test). (*G* and *H*) RH30 cells infected with a viral vector expressing shAVIL1, which targets the same sequence as siAVIL, had reduced proliferation measured by cell counting (*G*) and MTT (*H*). (*I*) Subcutaneous xenografts of RH30 cells infected with either viruses expressing shAVIL1 or a control sequence shCT ($n = 10$). All animals in the shCT group developed tumors, whereas the shAVIL1 group had only two small tumors. (*J* and *K*) Comparison of tumor weight (*J*) and volume (*K*) between the two groups. (*L*) Kaplan–Meier survival curve for the shCT and shAVIL1 groups. All the shCT animals died or reached the endpoint for tumor size limitation, whereas none of the mice in the shAVIL1 group did (one mouse was killed as a control when the first shCT mice were terminated) (two-sided Log-rank test). m-q RH30 cells stably expressing tet-inducible shAVIL or shCT were injected subcutaneously into nude mice. Animals were fed with doxycycline-containing or control water. Tumors were harvested (*M*). Weights (*N* and *P*) and volumes (*O* and *Q*) were measured. Data are presented as mean values ± SD in *C, G, H, J, K,* and *N–Q*. *P* values were calculated by standard two-tailed *t* test. $*P < 0.05$, $**P < 0.01$, $***P < 0.001$. n/s, not significant.

contrast, no significant difference was observed in MSC cells (Fig. 4 *G* and *H*). These findings support that a high level of AVIL expression is necessary for RMS cell growth and migration. We then tested the effect of AVIL silencing in vivo. Subcutaneous injection of RD cells infected with control shCT produced tumors in nine out of nine experiments. In contrast, injection of RD cells infected with shAVIL yielded only four tiny tumors in nine experiments (Fig. 4*I*). Significant differences were observed in tumor volume, weight, and animal survival (Fig. 4 *J–L*).

Conversely, in gain-of-function systems, overexpressing AVIL in cell lines, including MSC and RH4, resulted in a higher proliferation rate and migration (Fig. 5 *A–D*), supporting its role in promoting cell proliferation and migration.

AVIL Is a Bona Fide Oncogene in RMS. Finally, to test whether AVIL functions as a bona fide oncogene, we performed the classic oncogene test, the focus assay on NIH 3T3 cells (14). We observed significantly higher numbers of foci in cells transfected with AVIL than with an empty vector control (Fig. 5*E*). To examine the potential collaborative effect of AVIL with two major oncogenic pathways (P3F fusion and RAS) in RMS, we performed an oncogene cooperativity assay, where we introduced P3F or RAS alone, or in combination with AVIL overexpression. As shown in Fig. 5*E*, NIH 3T3 cells with RAS transfection resulted in a many-foci formation, while P3F overexpression did not produce a significantly higher number of foci than empty vector control. Impressively, overexpressing AVIL alone yielded a similar number of foci as RAS. In addition, combining AVIL with the two factors did not result in more foci than AVIL alone, but much more than P3F. These results support that AVIL is sufficient to trigger focus formation and is at least as powerful, if not stronger, than the known oncogenic factors at triggering the

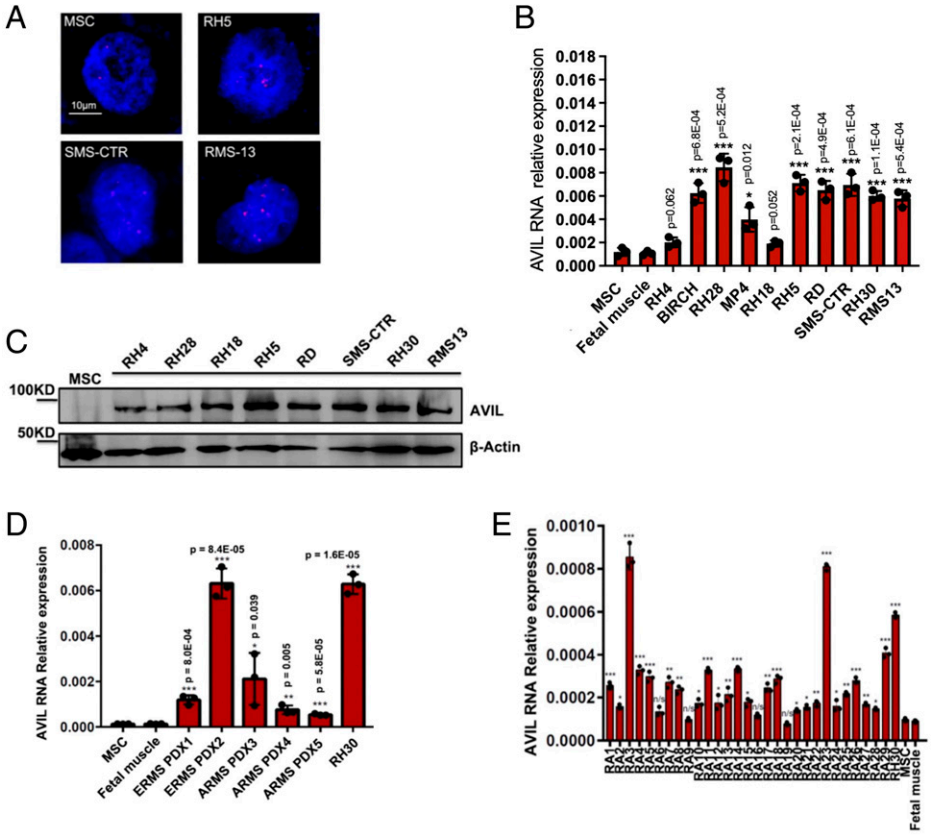

Fig. 3. AVIL is overexpressed in RMS. (*A*) FISH staining using an AVIL probe on MSC, RH5, SMS-CTR, and RMS13, showing that all three RMS lines have more than four dots, whereas MSC cells only two. (*B*) qRT-PCR measuring *AVIL* level relative to *GAPDH* among RMS cell lines. (*C*) Western blot with AVIL antibody comparing AVIL protein expression in MSC and RMS cell lines. (*D* and *E*) qRT-PCR measuring AVIL level relative to that of *GAPDH* among PDX samples (*D*) and clinical RMS samples (*E*). Data are presented as mean values ± SD in *B, D,* and *E*. *P* values were calculated by standard two-tailed *t* test. $*P < 0.05$, $**P < 0.01$, $***P < 0.001$.

escaping of contact inhibition. Consistently, overexpressing AVIL in MSC cells also resulted in a significantly higher number of foci (Fig. 5*F*).

Ultimately, it comes down to in vivo tumorigenesis to test whether a gene is a bona fide oncogene. Here, we found that overexpressing AVIL alone in MSC cells is sufficient to transform the cells in a subcutaneous xenograft model (Fig. 5*G*). In the same animals, the left flank was injected with MSC cells transfected with empty vector control (MSC/CT). In contrast, the right side was injected with MSC cells transfected with an AVIL overexpression vector (MSC/AVIL). Eight out of nine animals developed a large mass on the right side, whereas only one animal had a small mass on the left side. Consistently, the tumor volume and weight are significantly different between MSC/AVIL and MSC/CT (Fig. 5 *H* and *I*). We then confirmed the masses being actual tumors by histology (Fig. 5*J*). Similar to AVIL, MARS-AVIL overexpression resulted in more foci formations (*SI Appendix*, Fig. S7*A*) and can transform MSC cells in vivo (*SI Appendix*, Fig. S7 *B–E*).

AVIL May Be the Converging Node of Two Oncogenic Pathways. The fact that AVIL is overexpressed in both ARMS and ERMS cell lines as well as clinical samples made us wonder whether AVIL may function as a common node for both types of RMS, merging the two tumor-driving pathways. Consistently, the cooperative foci formation assays revealed that addition of P3F or RAS did not yield more foci than AVIL alone. We conducted a triplicate RNA-seq experiment comparing the gene expression in AVIL-overexpressed MSC cells vs. control MSC cells (*SI Appendix*, Fig. S8*A*). We noticed many targets of both P3F and RAS are differentially expressed (Fig. 6*A*). Indeed, gene set enrichment analysis (GSEA) analyses revealed the enrichment of PAX-FOXO1 gene expression signature that defines molecular classes and determines the prognosis of alveolar rhabdomyosarcomas (15), as well as a gene set found in mouse MSC cells expressing PAX-FOXO1 fusion (16) (Fig. 6*B*). Consistently, these differentially expressed genes were also overrepresented in the 76 genes recently reported as PAX3-FOXO1 targets using ChIP-Seq (17) (*SI Appendix*, Fig. S8b). Interestingly, a curated RAS gene signature was also enriched (Fig. 6*C*). We performed qPCR to measure 14 known downstream targets of PAX3 and PAX3-FOXO1, including *MYOD1* and FGFR4. Twelve were found to be significantly changed upon AVIL overexpression (Fig. 6*D*). Similarly, we chose 22 RAS downstream target genes for validation by qRT-PCR and confirmed 18 being induced or suppressed with AVIL significantly. To further confirm RAS pathway activation, we measured protein level changes of phosphorylated MEK1/2, and ERK1/2. In both MSC and RH4 systems, overexpressing AVIL enhanced the level of phosphorylated MEK1/2 and ERK1/2 (Fig. 6*E*). Conversely, silencing AVIL in RD cells resulted in reduced signal of both phosphorylated MEK1/2 and ERK1/2.

AVIL Activation May Be a General Oncogenic Pathway in Sarcomas. We noticed that the AVIL locus is frequently amplified in sarcoma (Fig. 7*A*). By qPCR, we found that *AVIL* RNA is also overexpressed in many other sarcoma cell lines, including

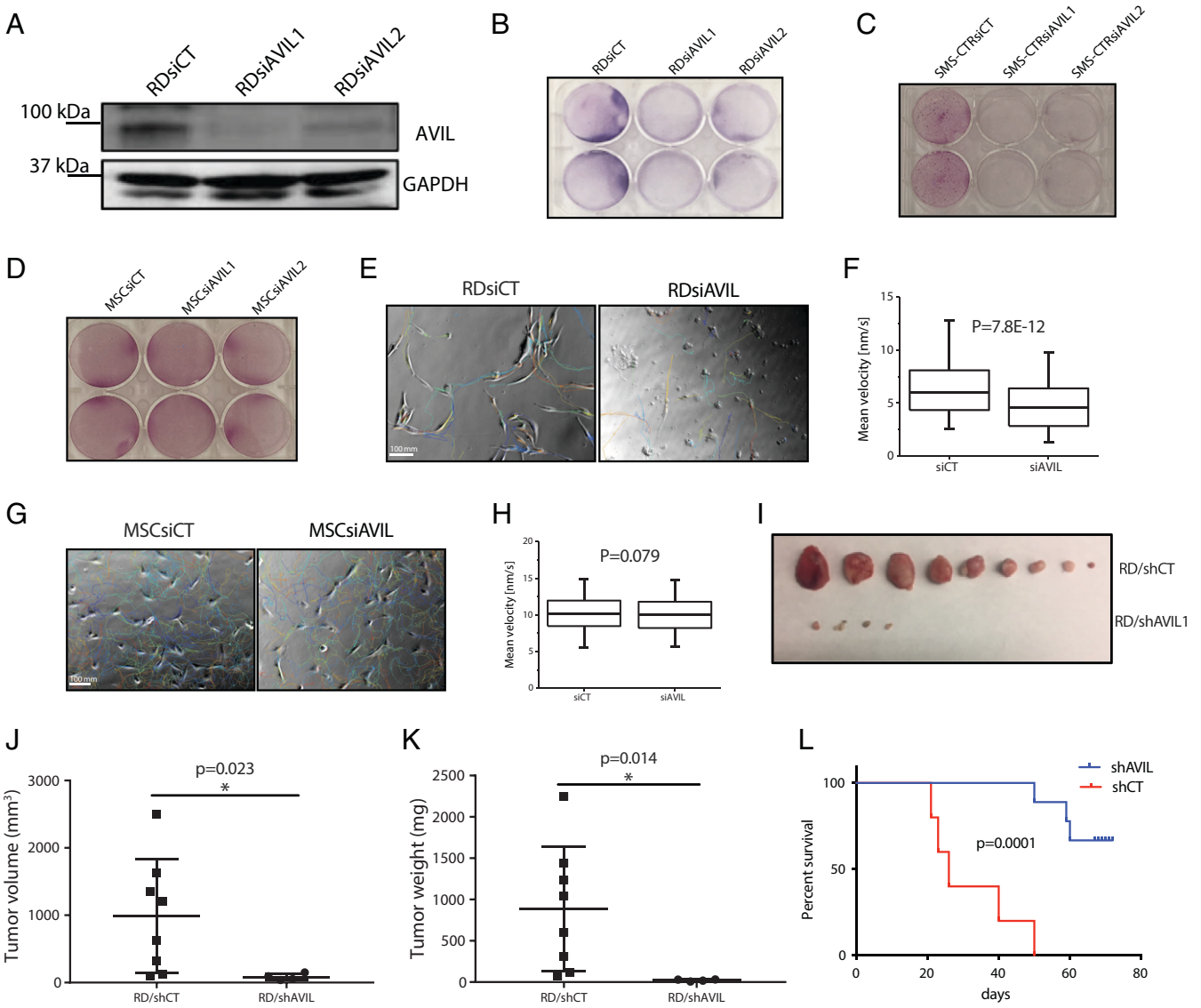

Fig. 4. AVIL overexpression is necessary for RMS tumorigenesis. (*A*) RD cells were transfected with two siRNA targeting AVIL (siAVIL1 and siAVIL2), or siGL2 as control (siCT). Western blot analysis demonstrated the knocking down of AVIL protein expression. (*B–D*) Crystal violet staining of RD (*B*), SMS-CTR (*C*), and MSC (*D*) cell cultures transfected with the same set of siRNAs as in *A*. (*E*) Live-cell imaging tracking individual cells of RD cells was observed over 24 h, starting 24 h after transection with either siCT (*Left*) or siAVIL1 (*Right*). Shown are representative images depicting the starting time point of the experiment with overlaid lines tracking the movement of individual cells. (*F*) Mean velocities of all cells tracked in the experiment depicted in *E* ($n > 150$ cells quantified per condition) (box, 25 to 75 percentile; whisker, 5 to 95 percentile; bar in the *Middle*, median) (two-sided Student's *t* test). (*G*) Live-cell imaging for MSC cells using the same setup as in *E*. (*H*) Quantification of velocities of all cells tracked in *G* ($n > 1{,}000$). (*I*) Xenografts of RD cells expressing shAVIL1 or control (shCT). The tumors were harvested at the end of the experiment and are pictured. (*J* and *K*) Tumor volume (*J*) and weight (*K*) comparison between the two groups. (*L*) Percent survival of the animals was plotted according to Kaplan–Meier analysis (two-sided Log-rank test). Data are presented as mean values ± SD in *J* and *K*. *P* values were calculated by standard two-tailed *t* test. $*P < 0.05$.

Ewing sarcoma, myxoid liposarcoma, desmoplastic small round cell sarcoma, clear cell sarcoma, osteosarcoma, and synovial sarcoma cell lines (Fig. 7*B*). Consistently, we found enrichment of Ewing family tumor signature (18) as well as EWS-FLI triggered Ewing sarcoma progenitor signature (19) (Fig. 7 *C* and *D*). These findings stimulated us to examine the expression of AVIL in The Cancer Genome Atlas (TCGA) sarcoma database for patient survival. Indeed, a higher level of AVIL expression is correlated with significantly worse clinical outcomes than the AVIL low group (Fig. 7*E*).

Discussion

A potent oncogene might use multiple mechanisms to misregulate its activity, which at the same time give credence to the gene being a critical player in tumorigenesis and malignancy. AVIL forms a fusion with a housekeeping gene MARS in the patient where RH30 and RMS13 were established. Its locus is amplified by copy number in another subset of RMSs. The rest of the majority likely use transcriptional and/or posttranscriptional mechanisms to up-regulate its expression at RNA and protein levels. In addition to RMS, we have found that AVIL is overexpressed in many other sarcoma types, including Ewing, synovial, osteosarcoma, and liposarcoma. These and our previous finding that AVIL plays a critical role in glioblastoma (GBM) (20–22) suggest that AVIL may be a general oncogene, not limited to a particular cancer type.

AVIL is overexpressed in RMS cell lines, PDXs, and clinical samples at RNA and protein levels regardless of their molecular categories of PAX3/7-FOXO1 fusion positive and fusion negative. Intriguingly, in the NIH 3T3 oncogene cooperativity assay, the combination of RAS or PAX3-FOXO1 with AVIL

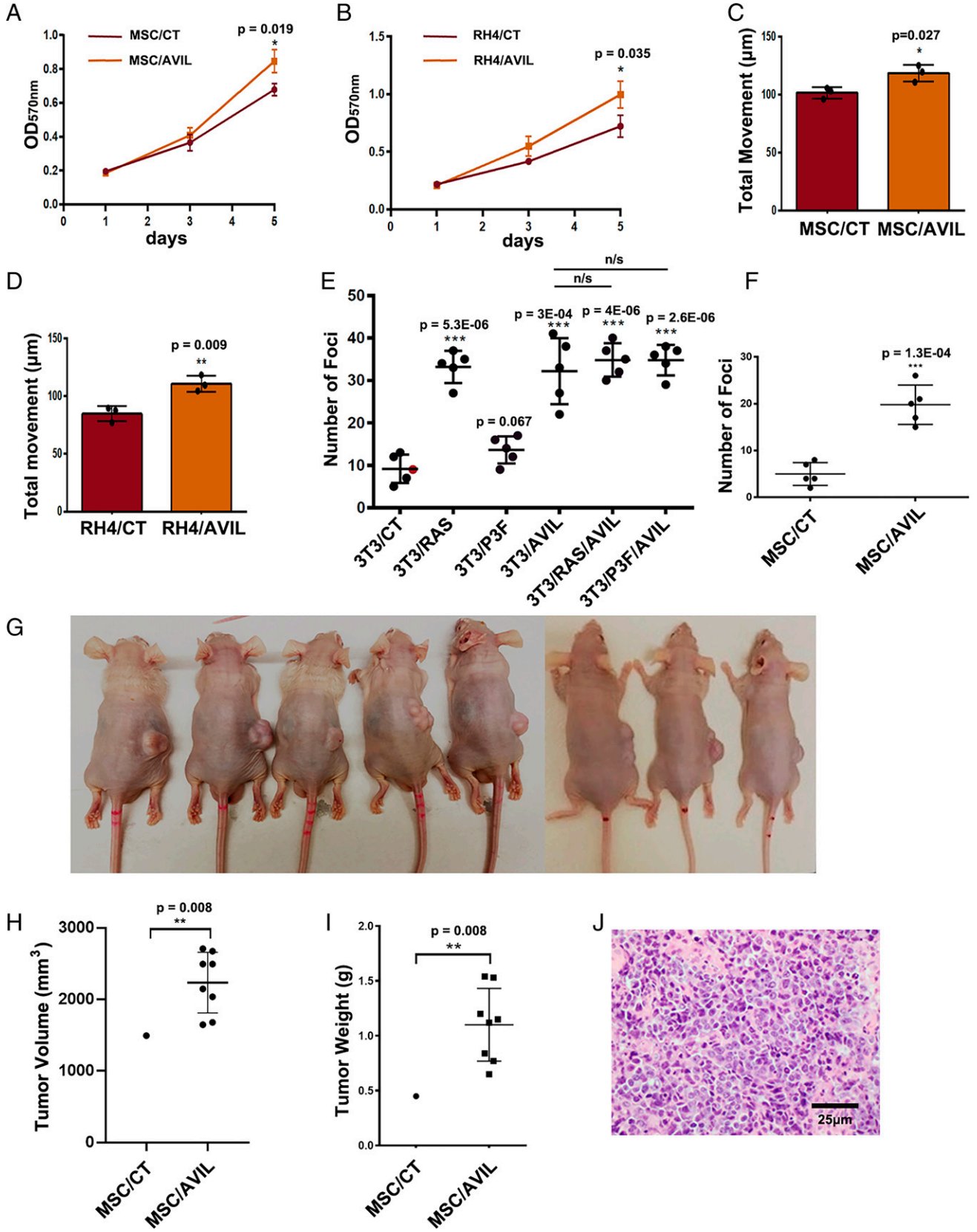

Fig. 5. AVIL is a bona fide oncogene in RMS. (*A* and *B*) Overexpressing AVIL in MSC (*A*) and RH4 (*B*) cells resulted in a higher proliferation rate measured by MTT. (*C* and *D*) Overexpressing AVIL in MSC (*C*) and RH4 (*D*) cells resulted in higher motility measured by wound healing. (*E*) Focus formation assay. Quantification of foci resulted from oncogene cooperation assays. NIH 3T3 cells were transfected with RAS and PAX3-FOXO1 with or without AVIL overexpression. Two-sided Student's *t* test was conducted. Each group is compared to the NIH 3T3 control group unless noted by a line; $n = 5$. (*F*) Focus formation assay. MSC cells were transfected with AVIL-expressing (AVIL) or control empty plasmid (CT). The quantitative difference of the foci number between the two groups was plotted; $n = 5$. (*G*) MSC cells expressing control plasmid (CT) or AVIL (AVIL) were injected subcutaneously into the flanks of immunodeficient mice. The same animals received CT on the left side and AVIL on the right. Representative images are shown. (*H* and *I*) Comparison of tumor volume (*H*) and weight (*I*) between the two groups. (*J*) Representative hematoxylin and eosin staining of the tumors harvested from the mice. Histology analysis revealed histologic features of neoplasms. Data are presented as mean values ± SD in *A*–*F*, *H*, and *I*. *P* values were calculated by standard two-tailed *t* test. $*P < 0.05$, $**P < 0.01$, $***P < 0.001$.

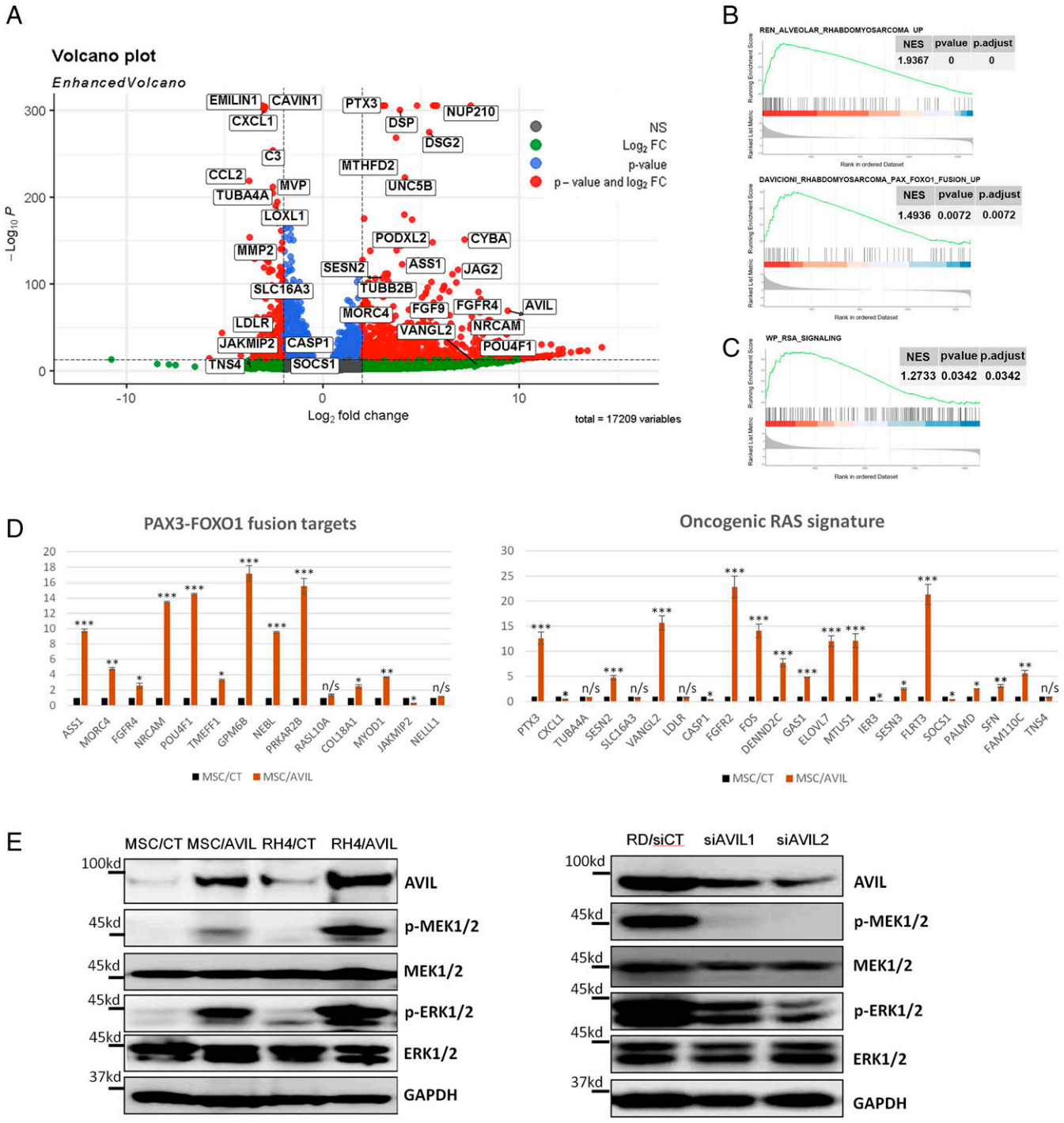

Fig. 6. AVIL regulates PAX3-FOXO1 and RAS pathways. (*A*) MSC cells expressing empty vector (CT), or AVIL were harvested. RNAs were extracted and sequenced at three different passages. Volcano plot of expression data rendered using the EnhancedVolcano library with Log2 fold change (FC) cutoff of abs|2| and padj < 0.01. Colors represent gene as nonsignificant (gray- "NS"), passing Log2 fold change cutoff only (green- "Log2 FC," padj cutoff only (light blue- "*P* value") or passing both Log2 fold change and padj cutoffs (red- "*P* value and Log2 FC"). Targets of PAX3-FOXO1 and RAS are highlighted. (*B*) GSEA analyses demonstrate the enrichment of PAX-FOXO1 gene expression signature that defines ARMS and its prognosis and a gene set found in mouse MSC cells expressing PAX-FOXO1 fusion. (*C*) Gene set for RAS signaling was also enriched. (*D*) qPCR validation for targets of PAX3-FOXO1 (*Left*) and RAS (*Right*). The levels of various transcripts were normalized against internal control GAPDH, then further normalized to that in MSC/CT. (*E*) Western blot measured the protein level changes of total and phosphorylated MEK1/2 and ERK1/2. Data are presented as mean values ± SD in *D* and *E*. *P* values were calculated by standard two-tailed *t* test. $^{*}P < 0.05$, $^{**}P < 0.01$, $^{***}P < 0.001$. n/s, not significant.

did not result in more foci than AVIL alone, suggesting that AVIL may be a node connecting oncogenic pathways for both categories of RMS. Supporting this hypothesis, the RAS pathway and PAX3-FOXO1 targets are both enriched with GSEA in MSC cells overexpressing AVIL. Both pathways are also confirmed to be activated upon AVIL overexpression based on qPCR and Western analyses, indicating that AVIL may lie in some common signaling axis in both types of RMS. Besides AVIL, sets of genes altered in fusion-negative RMS, including *MYOD* and *FGFR4*, have been noticed to also be targets of PAX3 and PAX3-FOXO1 (23), connecting the two pathways.

Alteration of the receptor tyrosine kinase/RAS/phosphoinositide 3-kinase (PI3K) axis affected 93% of RMS cases and appeared to hinge on the FGF and IGF receptor pathways (23, 24). It is

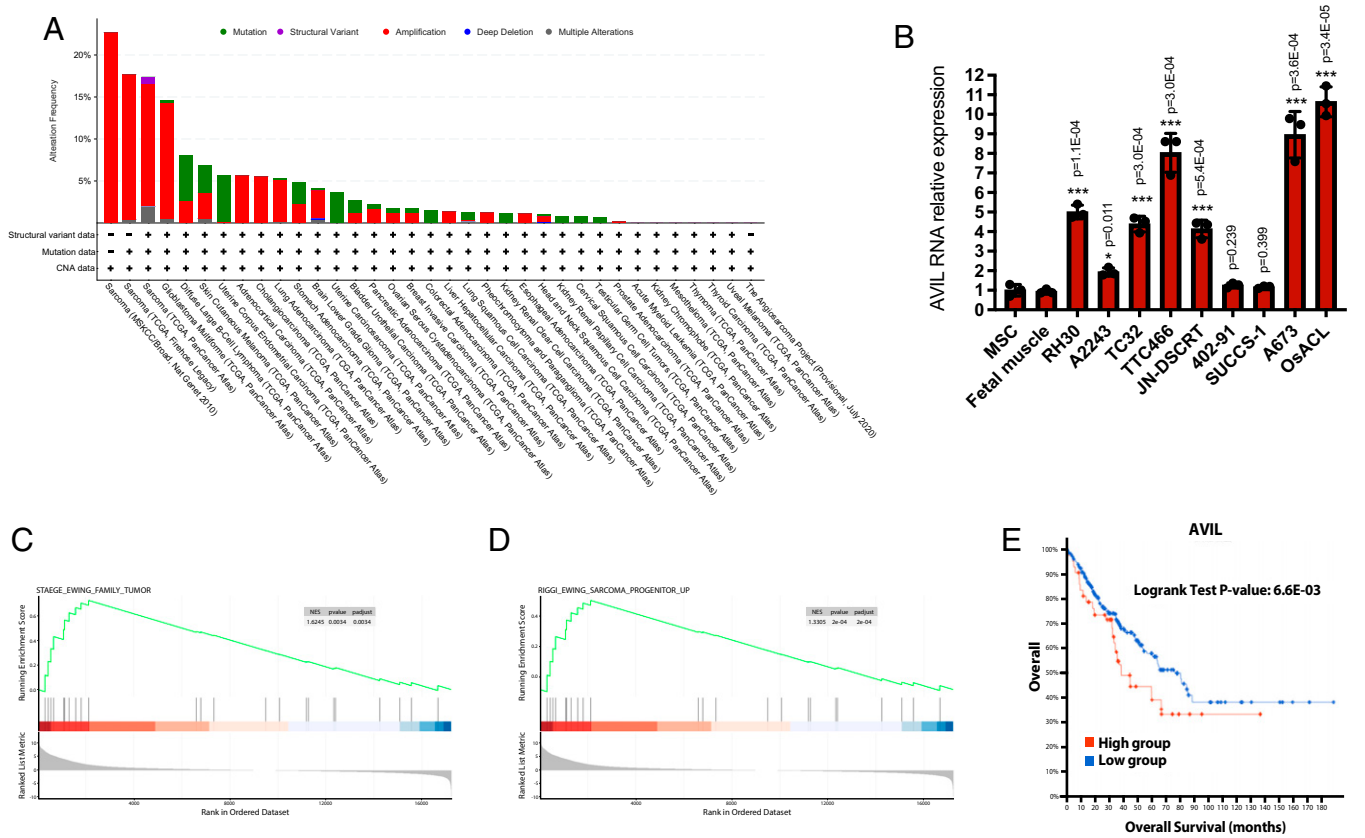

Fig. 7. AVIL is overexpressed in other sarcomas, and its expression correlates with worse clinical outcomes. (*A*) cBioPortal analysis on AVIL gene. (*B*) Relative *AVIL* expression against *GAPDH* was measured by qRT-PCR and compared in RH30, A673, TTC-466, and TC32 (Ewing sarcoma), 402–91 (myxoid liposarcoma), JN-DSRCT (desmoplastic small round cell sarcoma), SUCCS-1 (clear cell sarcoma), A2243 (synovial sarcoma), and OsACL (osteosarcoma) cells. (*C* and *D*) GSEA analysis showed enrichment of Ewing family tumor signature (*C*) and EWS-FLI triggered Ewing sarcoma progenitor signature (*D*). (*E*) Clinical analysis using TCGA sarcoma dataset. A two-class model stratified by AVIL showed that the high AVIL group has a shorter overall survival. Data are presented as mean values ± SD in *B*, and *P* value was calculated by standard two-tailed *t* test. *P* values in *E* were calculated with two-sided Log-rank test. ***$P < 0.001$.

known that activation of Ras and Rac plays a critical role in mediating downstream motility events, such as membrane ruffling and cell protrusion (25). Advillin encoded by *AVIL* regulates F-actin dynamics. Even though it is less studied, the same family member gelsolin has been shown to be a downstream effector of Rac, but at the same time affect Rac expression (26). Also gelsolin is evidently a downstream effector of the Ras-PI3K signaling pathway in cellular invasion (27). Likely, AVIL may reside on the feedback loop of Ras/Rac-PI3K pathways affecting both categories of RMS.

MARS-AVIL fusion is formed by chromosomal inversion and encodes an in-frame fusion protein. Together with PAX3-FOXO1, they are the few shared fusions in RH30 and RMS13, believed to be established from the same donor patient (10). The identical fusion junction sequence is seen in an image clone deposited in the human nonreference RNA database, with the source of rhabdomyosarcoma, suggesting that the fusion is likely to be present in a subset of RMS. However, in our collection of 29 RMS clinical samples, we did not detect this fusion, suggesting that it is a rare event. Phenotypically, like wild-type AVIL, MARS-AVIL transfection enhanced cell proliferation, migration, foci formation, and enabled MSC transformation in vivo. However, it likely has its unique function, as wild-type AVIL cannot rescue the effect caused by MARS-AVIL silencing. Additionally, RNA-seq of MSC cells expressing MARS-AVIL revealed distinctive profiles from that of MSC cells overexpressing AVIL, in that MARS-AVIL uniquely up-regulated about 217 genes, whereas AVIL induced the expression of 276 unique genes. A number of gene ontology terms such as embryonic organ and skeletal system morphogenesis are enriched in MARS-AVIL–regulated genes (*SI Appendix*, Fig. S9).

Methods

Clinical and PDX Samples. RNA of rhabdosarcoma patients were obtained from F.G.B. Cryopreserved cells for implantation and flash-frozen PDX samples were gifts from St. Jude Children's Research Hospital, Memphis, TN (13).

Statistics and Reproducibility. All the experiments were repeated at least three times unless otherwise noted. All quantitative data were presented as the mean ± SEM (SEM) or the mean ± SD (SD) as indicated in at least three independent experiments by Student's *t* test for between-group differences. Clinical prognosis was analyzed by the Kaplan–Meier method and Log-rank test. $P < 0.05$ was considered statistically significant.

Data Availability. RNA-seq data for MSC cells overexpressing AVIL and MSC control triplicates have been deposited into the Gene Expression Omnibus (GEO) database, under accession no. GSE180837. All other study data are included in the article and/or supporting information.

ACKNOWLEDGMENTS. We thank St. Jude Children's Research Hospital for providing the PDX models. H.L. was supported by National Cancer Institute (NCI) Grant R01CA240601. F.G.B. was supported by the Intramural Research Program of the NCI. The high-performance computing systems and services used in this work were provided by the Data Science Institute and the other Computation and Data Resource Exchange partner organizations at the University of Virginia.

1. D. M. Parham, D. A. Ellison, Rhabdomyosarcomas in adults and children: An update. *Arch. Pathol. Lab. Med.* **130**, 1454–1465 (2006).
2. D. Williamson *et al.*, Fusion gene-negative alveolar rhabdomyosarcoma is clinically and molecularly indistinguishable from embryonal rhabdomyosarcoma. *J. Clin. Oncol.* **28**, 2151–2158 (2010).
3. E. Davicioni *et al.*, Molecular classification of rhabdomyosarcoma–genotypic and phenotypic determinants of diagnosis: A report from the Children's Oncology Group. *Am. J. Pathol.* **174**, 550–564 (2009).
4. M. Laé *et al.*, Global gene expression profiling of PAX-FKHR fusion-positive alveolar and PAX-FKHR fusion-negative embryonal rhabdomyosarcomas. *J. Pathol.* **212**, 143–151 (2007).
5. E. R. Rudzinski *et al.*, Histology, fusion status, and outcome in metastatic rhabdomyosarcoma: A report from the Children's Oncology Group. *Pediatr. Blood Cancer* **64**, e26645 (2017).
6. M. E. Yohe *et al.*, Insights into pediatric rhabdomyosarcoma research: Challenges and goals. *Pediatr. Blood Cancer.* **66**, e27869 (2019).
7. P. W. Marks, M. Arai, J. L. Bandura, D. J. Kwiatkowski, Advillin (p92): A new member of the gelsolin/villin family of actin regulatory proteins. *J. Cell Sci.* **111**, 2129–2136 (1998).
8. Z. Xie *et al.*, Fusion transcriptome profiling provides insights into alveolar rhabdomyosarcoma. *Proc. Natl. Acad. Sci. U.S.A.* **113**, 13126–13131 (2016).
9. Z. Xie, H. Li, Fusion RNA profiling provides hints on cell of origin of mysterious tumor. *Mol. Cell. Oncol.* **4**, e1263714 (2016).
10. A. R. Hinson *et al.*, Human rhabdomyosarcoma cell lines for rhabdomyosarcoma research: Utility and pitfalls. *Front. Oncol.* **3**, 183 (2013).
11. R. L. Strausberg *et al.*; Mammalian Gene Collection Program Team, Generation and initial analysis of more than 15,000 full-length human and mouse cDNA sequences. *Proc. Natl. Acad. Sci. U.S.A.* **99**, 16899–16903 (2002).
12. G. Reifenberger *et al.*, Refined mapping of 12q13-q15 amplicons in human malignant gliomas suggests CDK4/SAS and MDM2 as independent amplification targets. *Cancer Res.* **56**, 5141–5145 (1996).
13. E. Stewart *et al.*, The Childhood Solid Tumor Network: A new resource for the developmental biology and oncology research communities. *Dev. Biol.* **411**, 287–293 (2016).
14. L. Raptis, A. Vultur, Neoplastic transformation assays. *Methods Mol. Biol.* **165**, 151–164 (2001).
15. E. Davicioni *et al.*, Identification of a PAX-FKHR gene expression signature that defines molecular classes and determines the prognosis of alveolar rhabdomyosarcomas. *Cancer Res.* **66**, 6936–6946 (2006).
16. Y. X. Ren *et al.*, Mouse mesenchymal stem cells expressing PAX-FKHR form alveolar rhabdomyosarcomas by cooperating with secondary mutations. *Cancer Res.* **68**, 6587–6597 (2008).
17. L. Cao *et al.*, Genome-wide identification of PAX3-FKHR binding sites in rhabdomyosarcoma reveals candidate target genes important for development and cancer. *Cancer Res.* **70**, 6497–6508 (2010).
18. M. S. Staege *et al.*, DNA microarrays reveal relationship of Ewing family tumors to both endothelial and fetal neural crest-derived cells and define novel targets. *Cancer Res.* **64**, 8213–8221 (2004).
19. N. Riggi *et al.*, EWS-FLI-1 expression triggers a Ewing's sarcoma initiation program in primary human mesenchymal stem cells. *Cancer Res.* **68**, 2176–2185 (2008).
20. Z. Xie *et al.*, A cytoskeleton regulator AVIL drives tumorigenesis in glioblastoma. *Nat. Commun.* **11**, 3457 (2020).
21. Z. Xie, H. Li, The discovery of AVIL as a *bona fide* oncogene in glioblastoma. *Mol. Cell. Oncol.* **7**, 1804309 (2020).
22. R. Cornelison, L. Marrah, D. Horter, S. Lynch, H. Li, Targeting AVIL, a New Cytoskeleton Regulator in Glioblastoma. *Int. J. Mol. Sci.* **22**, 13635 (2021).
23. J. F. Shern *et al.*, Comprehensive genomic analysis of rhabdomyosarcoma reveals a landscape of alterations affecting a common genetic axis in fusion-positive and fusion-negative tumors. *Cancer Discov.* **4**, 216–231 (2014).
24. B. Zhu, J. K. Davie, New insights into signalling-pathway alterations in rhabdomyosarcoma. *Br. J. Cancer* **112**, 227–231 (2015).
25. A. Malliri *et al.*, The transcription factor AP-1 is required for EGF-induced activation of rho-like GTPases, cytoskeletal rearrangements, motility, and in vitro invasion of A431 cells. *J. Cell Biol.* **143**, 1087–1099 (1998).
26. T. Azuma, W. Witke, T. P. Stossel, J. H. Hartwig, D. J. Kwiatkowski, Gelsolin is a downstream effector of rac for fibroblast motility. *EMBO J.* **17**, 1362–1370 (1998).
27. V. De Corte *et al.*, Gelsolin-induced epithelial cell invasion is dependent on Ras-Rac signaling. *EMBO J.* **21**, 6781–6790 (2002).